Uncooled and Passive 0.5-1.5 THz FPA Imager

Design and characterization of Focal Plane Array imager based on antenna-coupled MOSFET bolometers

Evgeny Shumaker, Dan Corcos, Noam Kaminsky, Danny Elad
IBM Haifa Research Lab,
Haifa University Campus, Carmel Mountain,
Haifa, Israel
E-mail: evgenysh@il.ibm.com

Thomas Morf, Bernhard Klein
IBM Zurich Research Lab,
Säumerstrasse 4,
Rüschlikon, Switzerland
E-mail : tmr@zurich.ibm.com

***Abstract*—Radiation in the "THz gap" holds great promise for numerous novel applications from navigation aids to medical imaging. An all-silicon antenna coupled MOSFET bolometer, realized in CMOS-SOI-MEMS process is intended to become a cornerstone of a novel focal-plane-array imager aimed at operation in the 0.5-1.5 THz range. The present article reports on the progress in design and characterization of this innovative sensor.**

Keywords— Microwave imaging, Microwave radiometry, Bolometers, Silicon on insulator technology, Micromachining.

I. INTRODUCTION

Known as “The Terahertz Gap” due to the lack of solid-state electronic devices, this last frontier of the electromagnetic spectrum extends from the upper edge of the microwaves to the far-infrared. Radiation in this region holds great promise for exciting new science and countless applications as its wavelengths are just right for large molecules spectroscopy and high resolution imaging capable of penetrating fog, dust, clothing and skin.

Millimeter-wave based imaging devices have already made their première in major EU and US airports, being employed for pre-boarding virtual strip searches of passengers. These systems are however active in nature, operate in the low millimeter-wave bands (which can barely be called THz) and are usually based on a very small array of sensors, thereby requiring significant scan times to form a single image of the person being inquired. A device suitable for large scale integration and capable of video frame-rate passive imaging is still to be demonstrated. Here passive stands for remote THz imaging not requiring any THz radiation source and relying solely on the very low-power natural THz radiation which is normally emitted from any body at above absolute zero temperature. Unfortunately, according to Plank-law, the power emitted in the THz range by objects at room-temperature is about three to four orders of magnitude smaller than in the 10 μm wavelength range, where the black body emission peaks. Passive THz imaging thus requires much higher sensitivity compared to passive IR imaging. Prior art passive THz imagers around 1 THz utilize small arrays of superconductor-based detectors cooled down to almost absolute zero temperature which unavoidably leads to prohibitively expensive and difficult to operate systems (e.g., cooling down to such temperatures in room environment takes several hours).

Therefore, a detector that can be used to detect high-frequency THz radiation but has much lower complexity and cost compared with existing superconducting solutions is highly desirable. Current research focuses on detectors using unconventional materials and concepts [1], such as detecting the radiation with semiconductor-based plasma devices (essentially, MOSFET based mixers [2]) and thermal antennas [3].

We propose to tackle the problem with an innovative Focal Plane Array technology, entirely integrated on-chip and based on antenna-coupled sensors, implemented in CMOS-SOI-MEMS technology. These sensors are being designed to provide passive imaging capabilities in the 0.5-1.5 THz range. The obvious benefit of this frequency range is the ability to obtain significantly higher resolution when compared to millimeter-wave systems while still availing substantial level of penetrability through most types of clothes [4].

Fig. 1 illustrates the proposed sensor. THz radiation is captured by light thermal mass but wideband antenna (shown here is a double cloverleaf antenna), with the signal being converted into heat by a termination resistor (shown in the inset). A MOSFET, adjacent to the resistor acts as a temperature sensor, indirectly detecting the THz radiation.

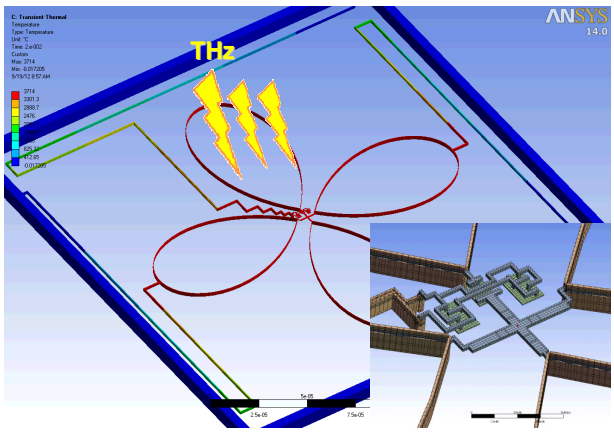

Fig. 1. Illustration of the antenna coupled MOSFET bolometer.

The research leading to the above results has received funding from the European Union Seventh Framework Program (FP7/2007-2013) under grant agreement no. [288442].

978-1-4673-5756-2/13/$31.00 ©2013 IEEE. *From the 2013 IEEE International Conference on Microwaves, Communications, Antennas and Electronic Systems (COMCAS 2013), Tel Aviv, Israel, 21-23 October 2013.*

This paper is outlined as follows: Section II briefly presents the system level considerations showing the viability of the proposed approach. Section III elaborates on challenges faced with in antenna design. Section IV provides preliminary characterization results of both the antenna and the sensor. Finally, Section V summarizes the results obtained so far.

II. SYSTEM LEVEL DESIGN

The list of specifications of any imaging system inevitably has to address the fundamental question of what needs to be recognized. It's generally accepted that this question is answered by interplay of two fundamental parameters of any imaging system, although the debate about the extent of their respective influence and whether they can be combined to yield a single figure-of-merit is still ongoing. These two are the on-target resolution and the system level sensitivity.

The issue of on-target resolution is dependent on the focusing mechanisms employed in a specific system and the volume available to incorporate those, but on a general level it would be safe to say that the issue of resolution is effectively the issue of the wavelength one has to work at – optics will at best to bring the system to the diffraction limit.

The issue of sensitivity is fundamentally more interesting as there is no apparent bound on this measure – state of the art is advanced whenever a smaller number is obtained, everything else being equal. For thermal imagers, to which the passive THz imagers definitely belong, the sensitivity is commonly stated in terms of Noise Equivalent Temperature Difference (NETD). It has been shown in [5] that quite successful recognition of concealed objects (based on THz range radiation) may be achieved with NETD better than 1 K.

The question of obtainable NETD of any imaging system (in any spectral range) really boils down then, to two simple questions: a) The signal (power) level available (for a given optics setup) at the sensor input and b) Noise level at the same input. These questions are addressed in the two following subsections.

A. *Received power*

In case of a Lambertian black-body, the power spectral density that falls on a detector of area A_D located behind optical setup having equivalent f-stop of $f_\#$ is (see [6] for details)

$$P\,d\nu = (L\,d\nu)\cdot\pi\cdot\tau_{opt}(\nu)\frac{A_D}{1+4f_\#^2} \qquad (1)$$

where $(L\,d\nu)$ is the scene irradiance given by the Planck law and $\tau_{opt}(\nu)$ is the transmittance of the optical system. For a body scanner scenario, in which an imaged object is a person wearing some clothes, the total power incident at the sensor is then

$$P = \int_{f_1}^{f_2} \tau_{cloth}(\nu)\cdot\tau_{air}(\nu)\cdot P\,d\nu \qquad (2)$$

where $\tau_{cloth}(\nu)$ and $\tau_{air}(\nu)$ are respectively the clothes and air transmittance coefficients. Extensive data on these have been compiled in [4] and [7].

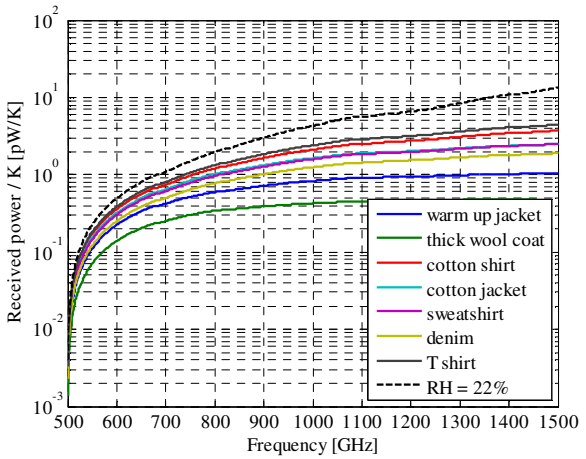

Fig. 2. Cumulative received power integral (starting 500 GHz) per 1K (around 300K) as received by a 250 um^2 antenna preceeded by $f_\# = 0.8$ optics.

Fig. 2 shows the resulting received power (by a 250 um^2 sensor preceded by $f_\#$ = 0.8 optics) expressed in pW per K of temperature difference (at baseline temperature of 300 K with 22% relative humidity (RH) of the environment and 2 m distance from the target). The black dashed line denotes the received power with no additional absorption due to clothing. Two important numbers stem from Fig. 2. First is that for bare body parts (such as palms and from the neck up) power levels of up to ~10 pW/K may be expected. However, body parts concealed by clothes will present signal power on the order of 1-2 pW/K, and that most of this power will occur at frequencies below 1 THz. Of course, this is only the power available to the sensor and not the actual received signal, which only stresses the imperative that the receiving element (an antenna in our case) must respond well in this frequency range (500 to 1000 GHz).

B. *Sensor noise*

Since a MOSFET acts as an electronic thermometer in the envisioned sensor (as has been first proposed in [3]), it plays a dominant role in determining the equivalent noise level at the input of the entire sensor. Translating the electrical noise of a MOSFET into incident signal power requires computing the sensors responsivity. Namely, by how much will the electrical characteristics of the transistor be altered if a sensor is irradiated with a unit power. The open-circuit voltage responsivity of a MOSFET based thermal sensor is given by

$$R_V(f_{FR}) = \eta\cdot\frac{1}{G_{th}}\cdot\left[1-e^{-\frac{1}{f_{FR}\cdot\tau_{th}}}\right]\cdot\frac{dV_{DS}}{dT}\quad\left[\frac{V}{W}\right] \qquad (3)$$

where η is the detector quantum efficiency (the fraction of incident power converted into heat), G_{th} (in W/K) is the thermal conductivity, τ_{th} the dominant thermal time constant and f_{FR} is the frame-rate. In the following calculations, η = 0.5

and G_{th} = 10^{-8} W/K, τ_{th} = 70 msec and f_{FR} = 1 Hz were assumed. dV_{DS}/dT was extracted from simulations based on IBM CSOI7RF PDK MOSFET models. Fig. 3 shows the resulting open-circuit voltage responsivity vs. bias current for a number of different MOSFET dimension sets (different width and length of the gate).

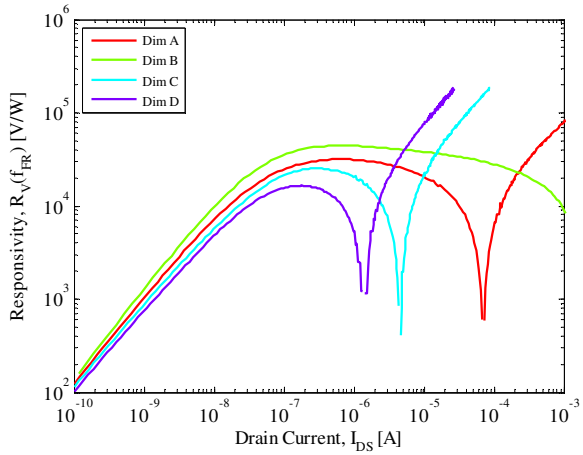

Fig. 3. Open circuit voltage responsivity at 1 Hz frame-rate vs. bias current.

Noise voltage spectral density was also simulated at open-circuits output using the above PDK models. The integrated (in 1 to 500 Hz range, as required by the read-out circuitry) noise voltage is shown in Fig. 4.

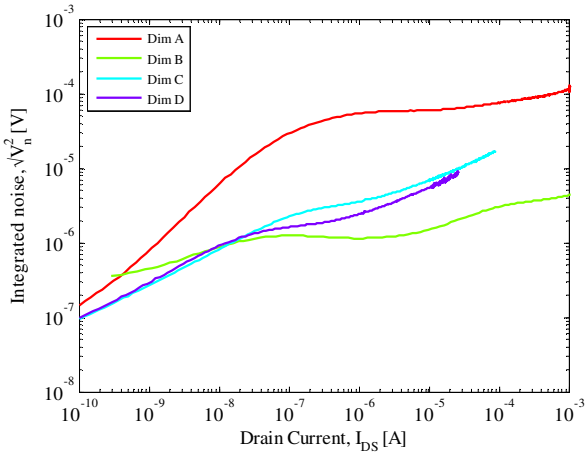

Fig. 4. Open circuit noise voltage (integrated in 1 to 500 Hz range) vs. bias current.

The noise equivalent power (NEP) can be easily inferred from these two numbers.

$$NEP = \frac{\sqrt{\langle V_n^2 \rangle}}{R_V(f_{FR})} \quad [W] \tag{4}$$

Fig. 5 shows the NEP for swept bias current. Stemming from the figure is the conclusion that currently, the best obtainable NEP is about 24 pW.

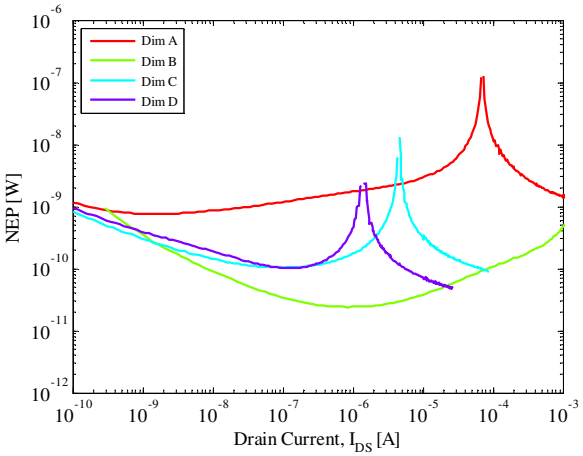

Fig. 5. Calculated NEP vs. bias current.

C. *Synthetic imaging*

The expected system NETD can now be readily calculated using a simple formula

$$NETD[K] = \frac{NEP[W]}{\text{Received power}\,[W/K]} \tag{5}$$

It can be easily fathomed that at current state of affairs, the best obtainable NETD is by far larger than the desired goal of 1 K. We have employed synthetic image generation algorithm to understand what kind of image quality may be expected at this level of noise and signal power at the sensor input.

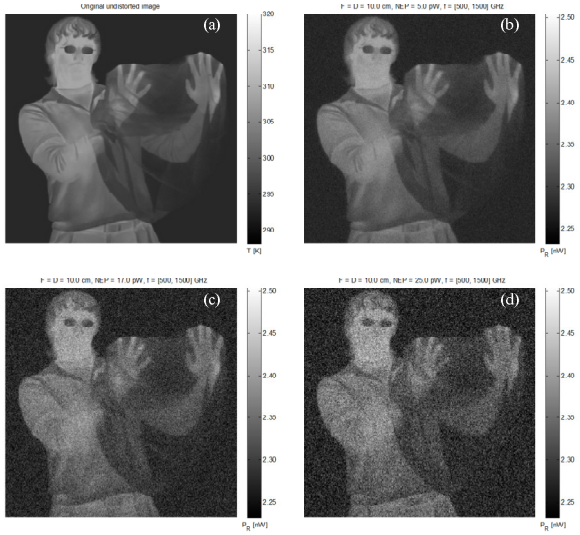

Fig. 6. (a) Original (undistorted) temperature map, received power map including optical point spread function taken for 500 – 1500 GHz frequency range with added noise, modeling NEP of (b) 5 (c) 17 and (d) 25 pW.

Fig. 6 visualizes the effect on image quality of varying NEP values applied to an original temperature map (taken with a high resolution IR camera) which has been distorted by finite

size optics, employing a method described in [8]. It's evident from Fig. 6 that optical NEP in excess of 17 pW renders smaller details indiscernible while NEP larger than 25 pW makes even the more obvious features contained in the image hard to see. Therefore, the current effort concentrates on means and methods of reducing/suppressing the 1/*f* noise which plays the dominant role in determining the output noise voltage of the MOSFET temperature sensor.

III. ANTENNA DESIGN

Several challenges are generally associated with such antennae. First and foremost, due to lack of amplification at higher THz frequencies, the received power is utterly dependent on the bandwidth in which the antenna is sensitive to the incident radiation. As concluded in Section II.a, it is absolutely imperative that the antenna responds well in the 500 to 1000 GHz frequency range. Second, the antenna must feature an as low as possible thermal time constant. Since detection process involves conversion of incident power into heat, time constants of this conversion process will determine the speed with which the image of the object can be refreshed. To obtain video frame-rate imagery, thermal time constants must be kept well-below 100 millisecond. Third count has to do with directivity – since the use of focusing optics is imperative to obtain the required resolution, radiated field overlap has to be tightly controlled all over the operation band. The relevant measure is the antenna FPA efficiency. Finally, since the antenna will be incorporated into a large focal plane array, mutual coupling has to be considered. Left unchecked, the undesired cross-talk will severely decrease the obtainable resolution.

The following section presents the simulation of the first and the third counts in the list above for a skirt antenna, as depicted in Fig. 7. Matching load resistors, responsible for dissipating the received energy into heat are located in the center.

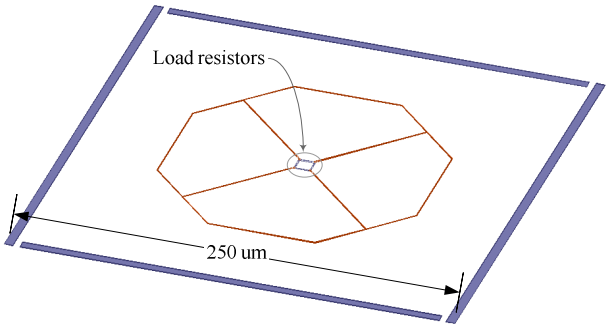

Fig. 7. View of the octagonal planar skirt antenna.

A. Absorption efficiency

A novel simulation methodology for accurately simulating absorption in terminated antennae based on modal reflection coefficients has been developed [9]. The resulting absorption efficiency (for the antenna in Fig.7) is shown in Fig. 8. Three different termination resistors have been experimented with, optimizing the total absorption integral.

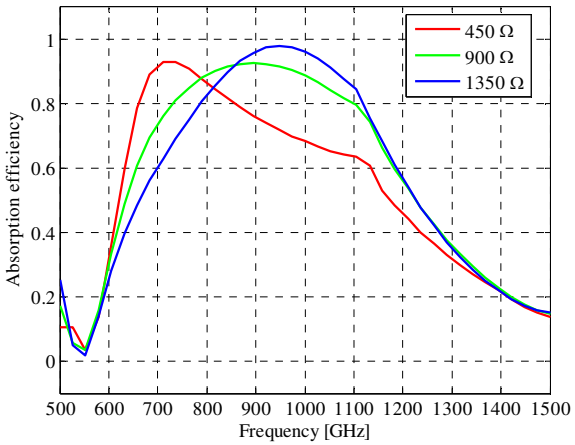

Fig. 8. Absorption efficiency of the octagonal planar skirt antenna for 3 different termination resistor values.

B. Antenna FPA efficiency

The FPA efficiency is determined by the overlap between the electromagnetic fields generated by the focusing optics and the electromagnetic fields generated by the antenna (usually assessed in transmission mode). If these fields overlap, than all of the energy that passes through the lens should be gathered by the antenna, thus providing 100% efficiency. In practice it is impossible to meet such a condition and usually the optics-antenna overlap is defined by 4 different sub-efficiencies [10] with the total coupling efficiency being a multiplication of them all [11].

Shown in Fig. 9 is the estimated total coupling efficiency of the octagonal planar skirt antenna (Fig. 7) vs. $f_{\#}$ of the focusing optics and plotted for 4 frequencies in the band of interest. Unfortunately, the efficiency peaks at unfeasibly low $f_{\#}$. More feasible $f_{\#}$ of about 0.8 will provide total efficiency > 0.5 across the band of interest (0.5 – 1.5 THz) with even higher values (> 0.7) at above 1.0 THz frequencies.

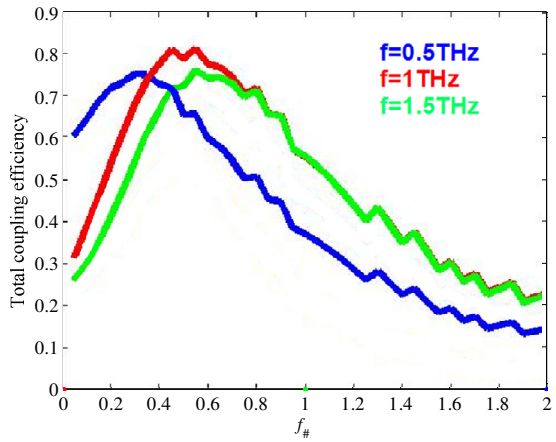

Fig. 9. Total coupling efficiency vs. $f_{\#}$ for different frequencies.

IV. CHARACTERIZATION RESULTS

Detailed description of the MEMS processing (following the standard silicon fabrication process) can be found in [12]. This section will review the preliminary characterization results in terms of two main measurements: the antenna directivity and total sensor responsivity.

A. *Antenna directivity*

Antenna directivity of an octagonal planar skirt antenna has been measured at 655 GHz and the obtained E-plane radiation pattern is shown in Fig. 10, depicting substantial agreement between the measurements and the simulation predictions.

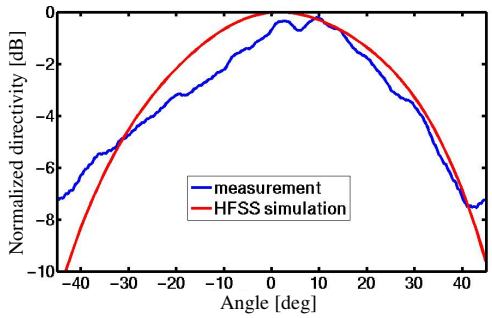

Fig. 10. E-plane antenna directivity vs. angle.

B. *Sensor responsivity*

Equation (3) shows that responsivity ultimately depends on the amount of thermal isolation of the pixel from the environment (expressed in terms of thermal conductance G_{th}). Good isolation required for a measured sample to reside in a vacuumed chamber in time of measurement. Unfortunately, vacuum was not available at the characterization facilities and so the correct responsivity could not be measured. Fig. 11 juxtaposes the current responsivity obtained in the air to a new simulation that takes this environmental condition into account.

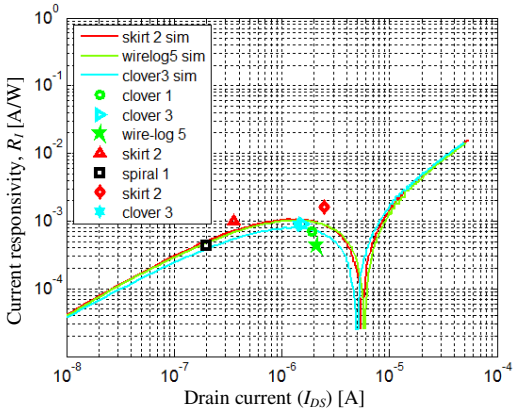

Fig. 11. Current responsivity vs. drain current.

Measurements for several antennae are shown in this figure, displaying good correspondence between the experimental results and the corresponding theoretical.

V. SUMMARY

A design of a FPA imager based on antenna-coupled MOSFET bolometers has been presented. Targeting a system level NETD of 1 K, the required system and sub-system level parameters have been obtained. Despite of currently falling short of the required benchmarks, thorough understanding of the key impeding issues has been obtained and substantial progress on design, manufacturing and characterization of these novel sensors has been achieved.

ACKNOWLEDGMENT

The authors acknowledge Prof. Ullrich Pfeiffer of the University of Wuppertal for availing his laboratory and assisting with experimental characterization of the manufactured sensors and Dr. Edward Cahoon of IBM Microelectronics Division for securing the silicon production area.

REFERENCES

[1] Y. Lee, Principle of Terahertz Science and Technology, Springer Science, LLC, New York, NY, 2009.

[2] H. Sherry, J. Grzyb, Y. Zhao, R. Al Hadi, A. Cathelin, A. Kaiser and U. Pfeiffer, "A 1k Pixel CMOS Camera Chip for 25 fps Real-Time Terahertz Imaging Applications", *Procceding of 2012 IEEE Int'l Solid-State Circuits Conf. (ISSCC 2012)*, San Francisco. CA, pp. 252-253, February 19-23, 2012.

[3] A. Svetlitza, I. Brouk, S. Bar-Lev, S. Stolyarova, Y. Nemirovsky, "The TeraMOS sensing pixel for monolithic passive uncooled THz imagers," *2012 International Conference on Optical MEMS and Nanophotonics (OMN)*, pp.123-124, 6-9 Aug. 2012.

[4] J.C. Dickinson, T.M. Goyette, A.J. Gatesman, C.S. Joseph, Z.G. Root, R.H. Giles, J. Waldman, W.E. Nixon, "Terahertz imaging of subjects with concealed weapons," *Terahertz for Military and Security Applications IV*, Edited by D.L. Woolard, R.J. Hwu, M.J. Rosker, J.O. Jensen, *Proceedings of the SPIE*, Volume 6212, pp. 62120Q (2006).

[5] C. Dietlein , A. Luukanen , F. Meyer , Z. Popovic and E. Grossman "Phenomenology of passive broadband terahertz images", *4th ESA Workshop on Millimetre-Wave Technology and Applications*, Espoo, Finland, 2006.

[6] H. F. Gilmore, "The Determination of Image Irradiance in Optical Systems," *Appl. Opt.* 5, 1812-1817, 1966.

[7] K.J. Linden, W.R. Neal, J. Waldman, A.J. Gatesman, A. Danylov, "Terahertz laser based standoff imaging system," *Proceedings of 34th Applied Imagery and Pattern Recognition Workshop,* pp.8-14, Dec. 2005.

[8] P. Y. Maeda, P.B. Catrysse and B.A. Wandell, "Integrating lens design with digital camera simulation", *Proceedings of the SPIE*, Volume 5678, pp. 48, 2005.

[9] N. Kaminski, D. Corcos, D. Elad, B. Klein, L. Kull, T. Morf, "A method for simulating the absorption of plane waves with FEM software tools", US 13/721088, filed January 2013.

[10] IEEE Standard Definitions of Terms for Antennas, IEEE Std 145-1993.

[11] C. C. Cutler, "Parabolic-Antenna Design for Microwaves," *Proceedings of the IRE*, vol.35, no.11, pp.1284-1294, Nov. 1947.

[12] T. Morf et. al, "Room-temperature THz imaging based on antenna-coupled MOSFET bolometer," *2013 IEEE 26th International Conference on Micro Electro Mechanical Systems (MEMS)*, pp.745-748, 20-24 January 2013.